# The Influence of Packing Densities and Surface Order on the Frictional Properties of Alkanethiol Self-Assembled Monolayers (SAMs) on Gold: A Comparison of SAMs Derived from Normal and Spiroalkanedithiols

Seunghwan Lee, Young-Seok Shon, Ramon Colorado, Jr., Rebecca L. Guenard, T. Randall Lee,* and Scott S. Perry*

*Department of Chemistry, University of Houston, Houston, Texas 77204-5641*

*Received July 13, 1999. In Final Form: November 15, 1999*

We report a comparative study of the structure and frictional properties of self-assembled monolayers (SAMs) generated by the adsorption of three homologous 17-carbon alkanethiols—heptadecanethiol, 2,2-dipentadecyl-1,3-propanedithiol, and 2-pentadecyl-1,3-propanedithiol—onto the surface of Au(111). The structural properties of these SAMs were characterized by atomic force microscopy, surface infrared spectroscopy, X-ray photoelectron spectroscopy, spectral ellipsometry, and wettability by water and hexadecane. The frictional properties of the SAMs were examined by friction force microscopy. The results demonstrate that the packing density and the related crystalline order of the hydrocarbon chains influence the frictional properties of organic thin films. The origins of the frictional differences measured from these films are discussed in terms of the structure of the films.

## Introduction

Self-assembled monolayers (SAMs) generated by the adsorption of alkanethiols on gold have been the subject of extensive research due to their facile preparation and characterization.[1,2] These SAMs afford molecular-level control over the structure and composition of organic thin films via the careful design, synthesis, and utilization of their specific alkanethiol adsorbates. Because SAMs consist of ultrathin and densely packed organic moieties on solid substrates, they represent ideal model systems for the study of lubrication at the molecular level. In the present investigation, we employ a molecular-level tool, atomic force microscopy (AFM),[3,4] to explore the specific relation between film packing density and interfacial friction of SAMs on gold derived from a series of structurally homologous alkanethiols.

Among the many factors believed to influence the frictional properties of organic thin films, effects due to packing density and film order (or crystallinity) remain poorly understood. Previous studies have shown that densely packed and well ordered SAMs exhibit lower friction than loosely packed disordered SAMs,[5−8] and have proposed that the presence of defects (e.g., free rotations about the C−C axes producing gauche defects) in the poorly ordered films are responsible for the higher friction.[5,6]

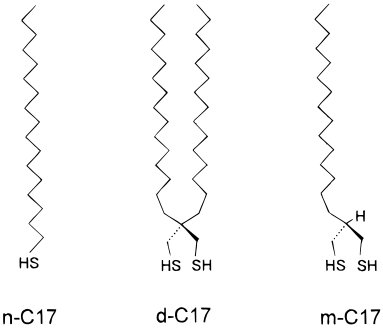


**Figure 1.** Schematic representation of the structures of the alkanethiols used in this study: (**1**) heptadecanethiol, (**2**) 2,2-dipentadecyl-1,3-propanedithiol, and (**3**) 2-pentadecyl-1,3-propanedithiol.

The proposed model argues that the defects provide additional excitation modes to efficiently absorb energy and thereby give rise to higher friction.

In the previous studies, the packing densities of the SAMs were indirectly controlled by varying the chain lengths,[5,6] anchoring groups,[6] underlying substrates,[6] or the chemical composition of the alkyl chains.[7,8] In the present work, we explore SAMs generated from a series of adsorbates that are designed to yield films in which the film structures (chain length and backbone structure) are held constant save for the packing densities.[9,10] The spiroalkanedithols illustrated in Figure 1, d-C17 and m-C17, can be used to form monolayers on Au(111) substrates in a manner analogous to normal alkanethiols such as n-C17.[9,10] Specifically, we examine the structural and related frictional properties of a series of three distinct 17-carbon adsorbates: heptadecanethiol, 2,2-dipentadecyl-1,3-propanedithiol, and 2-pentadecyl-1,3-propanedithiol. With this approach, any observed differences in frictional response can be traced to the different packing

* To whom correspondence should be addressed. T. Randall Lee E-mail: Trlee@uh.edu. Tel.: 713-743-2724. Scott S. Perry E-mail: Perry@uh.edu. Tel.: 713-743-2715.

(1) Ulman, A. *Chem. Rev.* **1996**, *96*, 1533.
(2) Carpick, R. W.; Salmeron, M. *Chem. Rev.* **1997**, *97*, 1163.
(3) Binnig, G.; Quate, C. F.; Gerber, C. *Phys. Rev. Lett.* **1986**, *56*, 930.
(4) Mate, C. M.; McCelland, G. M.; Erlandsson, R.; Chiang, S. *Phys. Rev. Lett.* **1987**, *59*, 1942.
(5) Xiao, X.; Hu, J.; Charych, D. H.; Salmeron, M. *Langmuir* **1996**, *12*, 235.
(6) Lio, A.; Charych, D. H.; Salmeron, M. *J. Phys. Chem. B.* **1997**, *101*, 3800.
(7) Overney, R. M.; Meyer, E.; Frommer, J.; Brodbeck, D.; Lüthi, R.; Howald, L.; Güntherodt, J.-J.; Fujihara, M.; Takano, H.; Gotoh, Y. *Nature* **1992**, *359*, 133.
(8) Meyer, E.; Overney, R.; Lüthi, R.; Brodbeck, R.; Howald, L.; Frommer, J.; Güntherodt, H.- J.; Wolter, O.; Fujihara, M.; Takano, M.; Gotoh, Y. *Thin Solid Films* **1992**, *220*, 132.
(9) Shon, Y. S.; Lee, T. R. *Langmuir* **1999**, *15*, 1136.
(10) Shon, Y. S.; Colorado, R., Jr.; Williams, C. T.; Bain, C. D.; Lee, T. R. *Langmuir* **2000**, *16*, 541.

10.1021/la9909345 CCC: $19.00 
Published on Web 01/19/2000

densities and the consequently different crystallinities of the corresponding films.

## Experimental Section

The three types of SAMs examined here were generated by adsorption from 1 mM solutions of heptadecanethiol, 2,2-dipentadecyl-1,3-propanedithiol, and 2-pentadecyl-1,3-propanedithiol onto gold substrates containing (111) terraces. Ethanol was employed as the solvent for the adsorption of heptadecanethiol, and for solubility reasons, isooctane was employed for the adsorption of 2,2-dipentadecyl-1,3-propanedithiol and 2-pentadecyl-1,3-propanedithiol. For simplicity, we refer to these compounds as n-C17 for heptadecanethiol, d-C17 for 2,2-dipentadecyl-1,3-propanedithiol and m-C17 for 2-pentadecyl-1,3-propanethiol (see Figure 1). The syntheses of the spiroalkanedithiols have been described in detail elsewhere.[9,10] For the AFM studies, the Au(111) substrates were prepared by annealing a gold wire (1 mm diameter) in a $H_2/O_2$ flame as described previously.[11,12]

We employed polarization modulation infrared reflection absorption spectroscopy (PM-IRRAS) to characterize the structural and conformational properties of the SAMs. For these experiments, the gold substrates (1 × 3 cm) were prepared by the thermal evaporation of chromium (ca. 100 Å) onto silicon wafers, followed by gold evaporation (ca. 2000 Å).[13] The PM-IRRAS spectra were collected using a Nicolet MAGNA-IR 860 Fourier transform spectrometer equipped with a liquid nitrogen-cooled mercury-cadmium-telluride (MCT) detector and a Hinds Instruments PEM-90 photoelastic modulator (37 kHz). The light was reflected from the samples at an angle of 80°. The spectra were collected over 256 scans at a spectral resolution of 4 $cm^{-1}$.

The thicknesses of the films were measured by spectral ellipsometry using a Rudolf Research Auto EL III ellipsometer equipped with a He−Ne laser operating at 632.8 nm and an angle of incidence of 70°. The films were further characterized by measuring the contact angles of water ($H_2O$) and hexadecane ($C_{16}H_{34}$, HD) using a Ramé-Hart model 100 contact angle goniometer. Further details of both types of measurements are available elsewhere.[9,10]

We obtained X-ray photoelectron spectra on freshly prepared samples using a PHI 5750 X-ray photoelectron spectrometer equipped with a monochromatic Al Kα X-ray source ($h\nu = 1486.7$ eV) incident at 90° relative to the axis of a hemispherical energy analyzer. All spectra were obtained with a pass energy of 23.5 eV, a photoelectron takeoff angle of 45° from the surface, and an analyzer spot diameter of 1.1 mm. Spectra were collected at room temperature and a base pressure of $2 \times 10^{-9}$ Torr for the following spectral regions and integration times: C 1s (1.67 min), S 2p (6.67 min), and Au 4f (0.67 min). Intensities were calculated with standard curve-fitting software using a Shirley background subtraction and Gaussian−Lorentzian curves. C 1s peaks were fit with a 100% Gaussian profile. Both S 2p and Au 4f peaks were fit with respect to spin−orbit splitting in the following manner: S 2p with two 80% Gaussian curves in a 1:2 area ratio split at 1.18 eV and Au 4f with two 65% Gaussian curves in a 3:4 area ratio split by 3.67 eV.[14]

The frictional properties of the SAMs were measured using a beam deflection atomic force microscope having a single tube scanner (0.5 inches in diameter and 1.0 inches in length). In this approach, light from a laser diode was focused onto the backside of a V-shaped microfabricated cantilever under which a sharp tip was attached. The deflection of the cantilever, which was driven by the interaction of the tip-cantilever assembly with the sample surface, was detected by a four-quadrant photodiode. RHK AFM 100 and RHK STM 1000 electronics were used in the control of the sample position and in data collection and processing.

Lateral and normal force maps were collected in a number of areas across the surface of each sample to evaluate the frictional properties of the SAMs.[15] Frictional forces were measured as a function of load by rastering the sample in a lateral direction while first increasing and then decreasing the applied load. In the 2D force maps, the *x*-scan represents a repeatedly scanned distance across the sample surface while the *y*-direction represents varying load. From these maps, the average kinetic frictional forces were plotted versus the average applied load during the line scan across the surface. Normal loads are expressed in force units derived from the manufacturer's (Digital Instruments, CA) specifications of the normal spring constant (0.58 N $m^{-1}$) of the tip-cantilever assemblies. Lateral forces were expressed in voltage units as measured from the photodiode detector without further conversion. While survey experiments were performed using several tip-cantilever assemblies, the results presented here for all samples were collected with the same tip-cantilever assembly to ensure precise comparison of the frictional data. The tip radii (typically ∼500 Å) were measured by imaging a reconstructed $SrTiO_3$ standard.[16] No evidence of tip wear was observed during any of the measurements described here. The scan length and speed were fixed at 1000 Å and 1 $\mu$m $s^{-1}$, respectively.

## Results and Discussion

**Film Structure and Packing Density.** The local structure of the SAMs generated by the adsorption of n-C17, d-C17, and m-C17 onto Au(111) were characterized using atomic force microscopy (data not shown). Large scale (1 $\mu m^2$) topographic images were collected by detecting the normal deflection of the cantilever as a function of sample position. The images of all SAMs were featureless on this scale except for the terraces and steps arising from the underlying gold substrate and were consistent with well-formed monolayers. On a smaller scale (∼50 × 50 $Å^2$), lateral force images, which were collected by detecting the lateral torsion of the cantilever as a function of sample position, were used to resolve molecular-level ordering within the films. For the n-C17 SAM, the well-known hexagonal structure ($\sqrt{3} \times \sqrt{3})R30°$ with respect to the Au(111) substrate[17] was routinely observed. In contrast, no periodic structures on a molecular scale consistent with the dimensions of the terminal groups of SAMs generated from the m- and d-C17 adsorbates were resolved in any of the samples examined (ca. 5 samples per adsorbate). We conclude from these measurements that the m- and d-C17 adsorbates exhibit little packing order on the Au(111) surface due to the presence of the dithiol headgroup and/or the quaternary carbon linkage.

The SAMs formed on thermally evaporated gold substrates were characterized by spectral ellipsometry, contact angle measurements, surface infrared spectroscopy, and XPS. Spectral ellipsometry revealed monolayer thicknesses of ∼20 Å for the n-C17 film, ∼19 Å for the d-C17 film, and ∼16 Å for the m-C17 film. Table 1 summarizes these data together with the data from the contact angle measurements.[9,10] The contact angles of the SAM generated from the m-C17 adsorbate (109° by $H_2O$ and 34° by HD) were substantially lower than those generated from the d-C17 (114° by $H_2O$ and 48° by HD)

(11) Kim, H. I.; Koini, T.; Lee, T. R.; Perry, S. S. *Langmuir* **1997**, *13*, 7192.

(12) Hayes, W. A.; Kim, H.; Yue, X.; Perry, S. S.; Shannon, C. *Langmuir* **1997**, *13*, 2511.

(13) Evaporated gold is polycrystalline with a predominant (111) orientation: Emch, R.; Nogami, J.; Dovek, M. M.; Lang, C. A.; Quate, C. F. *J. Appl. Phys.* **1989**, *65*, 79. Hallmark, V. M.; Chiang, S.; Rabolt, J. F.; Swalen, J. D.; Wilson, R. J. *Phys. Rev. Lett.* **1987**, *59*, 2879. Reichelt, K.; Lutz, H. O. *J. Cryst. Growth* **1971**, *10*, 103. Lee, M.-T.; Hsueh, C.-C.; Freund, M. S.; Ferguson, G. S. *Langmuir* **1998**, *14*, 6419.

(14) Moulder, J. F.; Stickle, W. F.; Sobol, P. E. *Handbook of X-ray Photoelectron Spectroscopy*; Chastain, J., King, R. C., Jr., Eds.; Physical Electronics, 1995.

(15) Perry, S. S.; Mate, C. M.; Somorjai, G. A. *Tribol. Lett.* **1995**, *1*, 233.

(16) Seiko S. S.; Moller, M.; Reavekamp, E. M. C. M.; Zandbergen, H. W. *Phys. Rev. B.* **1993**, *48*, 5765.

(17) Ulman, A. *An Introduction to Ultrathin Organic Films*; Academic: Boston, 1991.

**Table 1. Ellipsometric Thicknesses and Advancing Contact Angles of Water and Hexadecane of the SAMs**

| adsorbate | thickness[a] | $\theta_a^{H_2O}$ | $\theta_a^{HD}$ |
|---|---|---|---|
| m-C17 | 15.9 Å | 109 ± 1° | 34 ± 3° |
| d-C17 | 18.6 Å | 114 ± 1° | 48 ± 1° |
| n-C17 | 19.6 Å | 114 ± 1° | 47 ± 1° |

[a] Measured values were always within ±2 Å of the reported average value.

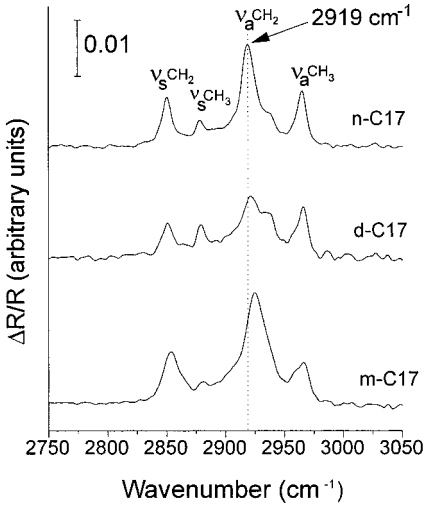


**Figure 2.** Polarization modulation infrared reflection absorption spectra (PM-IRRAS) of SAMs derived from heptadecanethiol (n-C17), 2,2-dipentadecyl-1,3-propanedithiol (d-C17), and 2-pentadecyl-1,3-propanedithiol (m-C17).

and n-C17 adsorbates (114° by $H_2O$ and 47° by HD). As a whole, these data are consistent with a model in which the latter two adsorbates generate well packed methyl-terminated SAMs; the m-C17 adsorbate, however, appears to generate SAMs that are loosely packed and/or that expose a substantial fraction of methylene moieties at the interface.[9,10]

Analysis by PM-IRRAS[18,19,20] revealed more detailed differences in the structural features of these SAMs. The frequency and bandwidth of the methylene asymmetric C−H stretch, $\nu_a(CH_2)$, are particularly sensitive to the degree of order (or crystallinity) of the films.[12,21,22,23] As seen in Figure 2, the $\nu_a(CH_2)$ peak of the m-C17 SAM appears at 2925 cm$^{-1}$, which is higher in frequency than that of both the d-C17 (2920 cm$^{-1}$) and the n-C17 (2919 cm$^{-1}$) SAMs. We thus conclude that the m-C17 adsorbate yields poorly ordered liquidlike SAMs.[24] Furthermore, the $\nu_a(CH_2)$ peak for the d-C17 SAM is slightly (but reproducibly) higher in frequency and somewhat broader than that of the n-C17 SAM. These observations suggest that the methylene backbones of the SAMs derived from the d-C17 adsorbate, although still well packed, are less crystalline than those derived from the n-C17 adsorbate. In future studies, a more detailed analysis of these data will seek to define the chain tilt and orientation in spiroalkanedithiol-based SAMs.

**Table 2. Integrated Photoelectron Intensities (Counts) and Relative Chain Densities**

| adsorbate | C 1s | S 2p | Au 4f | chain density from Au 4f | chain density from C 1s |
|---|---|---|---|---|---|
| m-C17 | 20664 | 2433 | 270912 | 64 ± 1% | 62 ± 2% |
| d-C17 | 25365 | 1546 | 235999 | 95 ± 1% | 94 ± 3% |
| n-C17 | 26538 | 1433 | 223060 | 100% | 100% |

Closely related to the molecular order within the films, the packing densities of the C17 SAMs were estimated by measuring the relative concentrations of carbon, sulfur, and gold in the interfacial region with XPS. This determination relied upon a quantitative calibration of photoelectron intensities arising from carbon-covered gold surfaces. First, we independently constructed reference curves for both the Au 4f and C 1s photoelectron intensities of SAMs generated from a series of normal alkanethiols of increasing chain length ($C_{12}$, $C_{14}$, $C_{16}$, $C_{18}$, and $C_{20}$). This procedure entailed plotting the natural log of the XPS integrated intensity versus the number of carbons in the alkyl chain to determine the attenuation properties of photoelectrons arising from these surfaces.[25] A least-squares analysis of the Au data gave an attenuation length for the Au 4f photoelectrons of 42 Å, in exact agreement with the value determined by Bain et al.[26] A logarithmic plot of carbon intensities versus chain length also yielded a linear dependence and verified that the C 1s photoelectron intensities also scaled with film thickness.[27] From these results, the relative carbon content of the C17 SAMs could be estimated through comparisons of both Au 4f and C 1s photoelectron intensities. The integrated intensities obtained from the three C17 SAMs are listed in Table 2 together with estimated chain densities. We note that the values for the n-C17 fell exactly on the calibration curves determined from even-numbered alkyl chains (i.e., exactly between the values obtained for C16 and C18 chains). Finally, working only from the number of carbons contained in each thiol unit (Figure 1), we estimate the relative density of carbon chains within the monolayer by comparing the carbon and gold intensities from the different SAMs. Assuming the $(\sqrt{3} \times \sqrt{3})R30°$ structure of the n-C17 represents a 100% packing on a Au(111) surface, the Au photoelectron intensities indicate a packing density of 95 ± 1% for d-C17 and 64 ± 1% for m-C17 with respect to n-C17. Alternatively, the C 1s intensities yielded packing densities of 94 ± 3% for d-C17 and 62 ± 2% for m-C17, with respect to n-C17.[28] In accord with the PM-IRRAS studies, these results are consistent with a loosely

(18) Anderson, M. R.; Evaniak, M. N.; Zhang, M. *Langmuir* **1996**, *12*, 2327.
(19) Gatin, M. R.; Anderson, M. R. *Vib. Spectrosc.* **1993**, *5*, 255.
(20) Golden, W. G.; Dunn, D. S.; Overend, J. *J. Catal.* **1981**, *71*, 395.
(21) Nuzzo, R. G.; Dubois, L. H.; Allara, D. L. *J. Am. Chem. Soc.* **1990**, *112*, 558.
(22) Nuzzo, R. G.; Fusco, F. A.; Allara, D. L. *J. Am. Chem. Soc.* **1987**, *109*, 2358.
(23) Bensebaa, F.; Voicu, R.; Huron, L.; Ellis, T. H. *Langmuir* **1997**, *13*, 5335.
(24) Porter, M. D.; Bright, T. B.; Allara, D. L.; Chidsey, C. E. D. *J. Am. Chem. Soc.* **1987**, *109*, 3559.

(25) Calibration curves were constructed for Au by plotting ln(Au 4f) versus the effective number of carbons and treating the attenuation due to the sulfur atom as equivalent to 1.5 methylene units (Harder, P.; Grunze, M.; Dahint, D.; Whitesides, G. M.; Laibinis, P. E. *J. Phys. Chem. B* **1998**, *102*, 426).

(26) Bain, C. D.; Whitesides, G. M. *J. Phys. Chem.* **1989**, *93*, 1670.

(27) To estimate relative chain packing densities from C 1s signals, we have assumed a linear behavior of C 1s intensities with chain length over the range of normal alkanethiols SAMs ($C_{12}$−$C_{20}$) used for calibration. Actually, C 1s intensities measured over a larger range of alkanethiol SAMs on gold ($C_6$−$C_{22}$) deviate from the expected linear model function $\ln(C_\infty - C_n) = \ln C_\infty - nd/(\lambda \sin \theta)$.[21] Au intensities, however, scale linearly with chain length and can consequently be used to reliably determine packing densities (Laibinis, P. E.; Bain, C. D.; Whitesides, G. M. *J. Phys. Chem.* **1991**, *95*, 7017). Therefore, the packing densities obtained from the C 1s signals should be regarded as approximations under the aforementioned assumption and are provided only in support of the packing densities determined from the Au 4f signals.

(28) Errors in the reported packing densities were determined by propagating the errors associated with the measured C 1s and Au 4f intensities (2% for C 1s and 1% for Au 4f, which were determined from the average and standard deviation of four measurements) throughout the calculations.

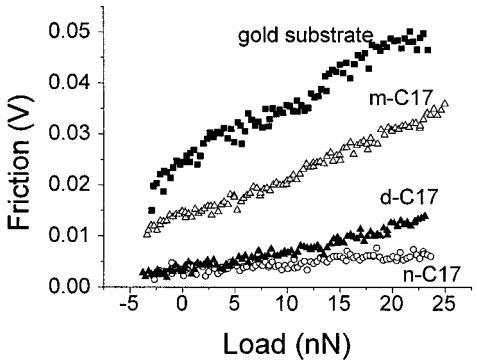


**Figure 3.** Representative friction−load maps in the increasing load regime for n-C17 (○), d-C17 (▲), and m-C17 (△) SAMs and a bare gold substrate (■). The frictional forces in the applied load regime (maximum ∼25 nN) and friction coefficients (the slopes of friction−load maps) increase in the following order: bare gold ≫ m-C17 ≫ d-C17 > n-C17.

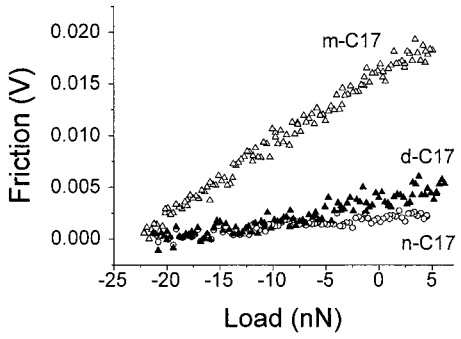


**Figure 4.** Representative friction−load maps in the decreasing load regime for n-C17 (○), d-C17 (▲), and m-C17 (△) SAMs. The pull-off force is indicated by the magnitude of the negative load experienced by the tip-cantilever assembly at the moment of separation from the film.

packed liquidlike structure for the hydrocarbon chains of m-C17 SAMs.

When taken together, the imaging studies by AFM, the film thicknesses determined by ellipsometry, the contact angle measurements, the PM-IRRAS data, and the estimation of the packing densities by XPS all support a model in which the monolayer films differ as follows with regard to the packing density and crystalline order of their hydrocarbon chains: n-C17 > d-C17 ≫ m-C17. Since the m-C17 adsorbate was synthetically designed to yield SAMs having approximately half the number of alkyl chains of both the n-C17 and the d-C17 SAMs, the observed low packing density and poor crystallinity were anticipated.[10]

**Frictional and Adhesive Properties of the SAMs.** The frictional properties of the SAMs generated from n-C17, d-C17, and m-C17 SAMs and bare gold substrates were measured through the acquisition of the friction-load data; representative friction-load plots are presented in Figure 3. The kinetic frictional forces shown here represent only those obtained under increasing applied load. To ensure a statistically valid comparison, the measurements were repeated several times in varying order, for a number of different sets of samples, each set utilizing the same tip-cantilever assembly. Although subtle differences were observed in the frictional responses of a given sample, the relative frictional properties of the SAMs were consistently distinguishable as in Figure 3. These data indicate that the frictional response of the hydrocarbon films can be ranked as follows: n-C17 < d-C17 ≪ m-C17. The relative frictional properties of the monolayer films mirror the trends in packing density and crystalline order of the films described above. Therefore, the predominant conclusion of this work is that, in the absence of changes in the *chemical* structure of an interface, the local packing and density of chemical moieties directly influences the frictional response of the interface. In particular, we find that densely packed or crystalline monolayer films of hydrocarbon chains exhibit lower friction as compared to loosely packed or liquidlike monolayers of the same composition.

The friction-load plots of these SAMs provide some insight into the origin of the differences in their frictional properties. As shown in Figure 3, the difference between the friction-load maps of n-C17 and d-C17 SAMs lies in the rate of increase of the kinetic frictional forces as a function of applied load. Similar static frictional forces upon initial contact between the tip and the films were observed for these two SAMs (data not shown). In contrast, the m-C17 film exhibited not only a higher kinetic frictional response over the entire range of increasing applied load (see Figure 3), but also a higher static frictional force upon initial contact.

While the n-C17 and d-C17 films differed from the m-C17 in terms of the friction measured upon initial contact and the rate of increase of friction with load, similar adhesive forces were observed among all three films. The degree of interfacial adhesion between the tip and the SAMs is seen in the magnitude of the pull-off forces during sliding, which were measured while decreasing the applied load (Figure 4). For these experiments, the maximum applied loads were constrained to no more than ∼5 nN to minimize deformation of the films, even if solely elastic in nature.[5,29] Despite clear differences in the frictional responses observed during the loading process (Figure 3), the value of the negative load at which the tip pulls off the surface (the pull-off force)[30] was similar for all three SAMs (see Figure 4). The JKR theory of adhesion mechanics dictates that this similarity in pull-off forces, measured with the identical tip, arises from similarities in the interfacial free energy.[30] The similarity in interfacial free energies is consistent with the similar chemical nature of these hydrocarbon films, which give rise to predominantly van der Waals forces across the interface.

In light of the similar adhesive properties, the observed frictional differences must arise from additional interaction mechanisms between the tip and the films. We believe that several interrelated structural phenomena are responsible for the frictional differences in these hydrocarbon films. The first issue involves the area of contact between the tip and the hydrocarbon film. As established through the XPS measurements, the m-C17 film possesses a significantly lower packing density than the other two C17 films. As a result, one would expect a lower elastic modulus (K) for the m-C17 film as compared to the two wellpacked films. A lower modulus would in turn give rise to an increased area of contact between the tip and the m-C17 film at any given load. As the friction force is equal to the shear strength times an area of contact, the lower elastic modulus will produce a greater frictional response for the loosely packed film. We note previous predictions and observations that the elastic modulus of a material will influence the area of contact *but not the interfacial pull-off force* (Figure 4).[30]

In addition to the standard concept of the area of contact, we propose that an effective area of contact, reflecting the number of atomic contacts that fall within the standard

(29) Liu, G.-Y.; Salmeron, M. *Langmuir* **1994**, *10*, 367.
(30) Israelachvilli, J. *Intermolecular and Surface Forces*; Academic: London, 1992; pp 326−329.

area of contact, is also related to observed frictional differences. For a more liquidlike film structure as in the case of the m-C17 film, there exists the possibility of a greater degree of contact along the backbone of the chain, as a result of either enhanced tip penetration or orientation of the hydrocarbon chains. Because the length of a C−C bond (1.54 Å) is substantially shorter than the distance spanned by the terminal methyl groups in normal SAMs on gold (4.99 Å), the van der Waals interactions between an AFM tip and the hydrocarbon backbones of loosely packed SAMs are likely to be greater per unit area than those between an AFM tip and the terminal methyl groups of well packed, well ordered SAMs. Thus, for the liquidlike m-C17 SAM, the van der Waals interactions while sliding across or through the film should be greater than that for either the n-C17 SAM or the d-C17 SAM. We propose that these additional van der Waals interactions give rise to the observed higher static and kinetic frictional responses for the m-C17 SAM by increasing the shear strength ($\tau$)[31] per unit area of contact. While this type of enhancement can plausibly occur for the loosely packed m-C17 SAM over the entire range of applied loads, enhancement for the d-C17 SAM should occur only at relatively high applied loads, where film deformation is likely to occur.[5,29] The data in Figure 3 are consistent with these interpretations.

We can also interpret the greater frictional response of the d-C17 and m-C17 films in terms of a previously reported model[5,6] in which less densely packed or more disordered films possess a greater number of channels of energy dissipation. These channels comprise local deformations within the films (local C−C bond rotations and the accompanying trans-gauche conformational changes) that absorb energy during the sliding process and thus give rise to higher frictional forces. As indicated by the PM-IRRAS measurements of these films, the m-C17 film possesses a lower degree of conformational order and thus a greater number of gauche defects within the unperturbed film with respect to the well packed n-C17 monolayer.[12,21,22,23] Moreover, the formation of a disproportionately greater number of defects would also be expected upon sliding within such an environment. A similar but less pronounced effect would be expected in the d-C17 monolayer that is fairly well packed (Table 2), but possesses low crystallinity.

As in real thin film systems, the structural phenomena of these model thin films are obviously interrelated. Based upon the present data, we believe that all of the mechanisms discussed here can plausibly give rise to the observed frictional differences. In addition, we believe that this collective model is also applicable to the observations by Xiao et al.[5] and Lio et al.[6] in which the frictional responses of poorly ordered short-chain SAMs of alkylsilanes on mica are greater than those of more ordered long-chain alkylsilane SAMs. Additional experimental work, when combined with theoretical techniques such as molecular dynamics simulations of sliding at hydrocarbon interfaces,[32] are likely to offer further insight into the molecular origin(s) of friction and lubrication in these and related hydrocarbon systems.

## Conclusions

These studies have demonstrated that the frictional properties of self-assembled monolayer films are directly influenced by their packing density and crystalline order. These conclusions were reached in a unique fashion through the synthetic design of thiol molecules that have been used to produce SAMs of the same chain length, but different packing densities. Specifically, we find that loosely packed and disordered SAMs exhibit higher interfacial friction than those that are well packed and highly ordered. We propose that the hydrocarbon chains of liquidlike SAMs have the capacity to interact more strongly with the contacting probe tip through an enhanced area of contact and increased van der Waals interactions compared to crystalline SAMs. The increased interactions strengthen the shear force per unit area and thereby give rise to a higher frictional response. Furthermore, sliding within loosely packed films likely dissipates greater amounts of energy through the excitation of molecular deformations, which can also give rise to a higher frictional response.

**Acknowledgment.** We thank the National Science Foundation for grants DMR-9700662 and CHE-9625003 (CAREER Award to T.R.L.) and the Robert A. Welch Foundation for grant E−1320. We thank Professor Colin Bain for helpful advice regarding the XPS analyses. We also thank our colleague Hyun Kim for his generous advice and assistance. This work made use of MRSEC Shared Experimental Facilities supported by the National Science Foundation under Award Number DMR-9632667.

LA9909345

(31) The force of friction is the shear strength of an interfacial contact times the area of contact (Bowden, F. P.; Tabor, D. *Friction and Lubrication of Solids: Part II*; Oxford University: London, 1964).

(32) Tutein, A. B.; Stuart, S. J.; Harrison, J. A. *J. Phys. Chem. B* **1999**, *103*, 11357.